Transient behaviours of float zones in μ-g and 1-g environments

Hussein Bazzi
Faculty of Engineering, Université de Sherbrooke, Sherbrooke, Québec, Canada
Cong Tam Nguyen
School of Engineering, Université de Moncton, Moncton, New Brunswick, Canada
Nicolas Galanis
Faculty of Engineering, Université de Sherbrooke, Sherbrooke, Québec, Canada

Received September 1998
Revised December 1999
Accepted January 2000

Keywords *Transient flow, Laminar flow, Boundary conditions, Heat*

Abstract *This work is concerned with the problem of the transient behaviours of the axisymmetric thermocapillary laminar flow occurring inside a half zone subjected to a variable thermal boundary condition during a heating process. The molten liquid with its deformable free surface is considered incompressible with constant physical properties except for its density in buoyancy forces where Boussinesq's approximation has been applied. The system of governing equations has been successfully solved by using the modified-SIMPLE method, while the instantaneous position of the free surface was determined by employing a special procedure. Numerical simulations have been carried out for both $NaNO_3$ and Silicon float zones operating under 1-g and μ-g conditions. The transient behaviours as well as the influence of the Marangoni number and the aspect ratio have been investigated.*

Nomenclature

A = aspect ratio, $A = R_0 / H$
Bd = dynamic Bond number, $Bd = \rho g \beta H^2 / | \partial \sigma / \partial T |$
Bs = static Bond number, $Bs = \rho g H^2 / \sigma$
Ca = capillary number, $Ca = | \partial \sigma / \partial T | \Delta T / \sigma$
C_p = specific heat of the fluid
H = height of the half zone
Ma = Marangoni number, $Ma = | \partial \sigma / \partial T | \Delta T H / \mu \kappa$
P = dimensionless pressure
Pr = Prandtl number, $Pr = C_p \mu / \lambda$
R, Z = dimensionless radial and axial coordinates
Re_{th} = thermocapillary Reynolds number, $Re_{th} = | \partial \sigma / \partial T | \Delta T H / \mu v = Ma / Pr$
Ro = radius of the zone
t, T = dimensional and dimensionless temperature
V_R = dimensionless radial velocity component
V_Z = dimensionless axial velocity component

The authors wish to thank the Natural Sciences and Engineering Research Council of Canada, the Ministry of Intergovernmental and Aboriginal Affairs of New Brunswick, the "Ministère de l'Éducation du Québec" and the Faculty of Graduate Studies and Research of the "Université de Moncton" for financial support to this project. Thanks are also due to the School of Engineering of the "Université de Moncton" for computing facilities and to Mrs. Dorine Léger for her efficient typing of this manuscript.

λ = thermal conductivity of the fluid
κ = the thermal diffusivity,
β = thermal expansion coefficient
μ = dynamic viscosity,
ν = kinematic viscosity
ρ = the density of the fluid
σ = surface tension of the liquid-vapor interface
τ = dimensional time
τ^* = dimensionless time

Introduction

The zone melting technique, as invented by Pfann (1966), has become a very popular mean today to produce high quality crystals, mainly because of its minimum risk of contamination. Experimental observations have shown that even under the condition of strongly reduced gravity, the presence of the thermocapillary flow – which results from a temperature gradient on the free surface – perturbs considerably the internal thermal field and thus, in turn, may affect greatly the crystallization process (Schwabe *et al.,* 1978, 1979a, 1982, 1989, 1990; Schwabe and Scharmann, 1979, 1983, 1984; Preisser *et al.,* 1983; Chun, 1980; Chun and Wuest, 1979, 1981, 1982, 1983). A comprehensive review of previous works in the domain may be found in Schwabe (1988) and Wilcox (1991).

The effects caused by the thermocapillary flow on the thermal field as well as the flow structure inside a float zone have also been studied numerically. Since the pioneer works by Chang and Wilcox (1975, 1976), there exist a considerably large amount of studies dealing with the hydrodynamic and thermal aspects of a float zone (see in particular, Kozhoukharova and Slavchev, 1986; Slavchev and Kojukharova, 1984; Saghir and Rosenblat, 1990; Saghir, 1998; Saghir *et al.,* 1992; Duranceau and Brown, 1986; Lan and Kou, 1990; Lan *et al.,* 1990; Kobayashi, 1988; Nguyen *et al.,* 1995a). These studies, although they have given considerable insights into the hydrodynamic and thermal behaviours of float zones operating under various gravity conditions, were concerned only with the steady-state regime. Since the dynamical crystallization process (formation and growth of dendritic structure and dislocations, ...) depends strongly on the temporal evolution of the temperature field within the float zone (see for example, Takao (1985) and Jordan *et al.* (1980)), the knowledge of the transient behaviours of the latter during the heating duration are, therefore, of crucial importance. Unfortunately, there exist only very few studies dealing with this aspect. With regard to the cylindrical float zone which is under consideration here, one should mention Saghir *et al.* (1992) who have successfully studied numerically the transient problem of a Silicon oil half zone on Earth condition where prescribed temperatures of both disks change with time. Their results of the internal flow and thermal field, as obtained for some specific "pseudo-steady-states" (i.e. with constant ΔT between the disks), seem to agree very well with their own experimental data. Rupp *et al.* (1989) and Kazarinoff and Wilkowski (1990) have considered the transient behaviour of a GaAs half-zone and a Silicon full-zone, respectively. However their works were concerned with the oscillatory flow structure under critical heating condition. In a recent work, Nguyen *et al.*

(1995b) have studied numerically the transient hydrodynamic and thermal behaviour of a float zone operating under 0-g condition. The structure of the internal flow field as well as the influence of key parameters have been thoroughly studied. In particular, the flow structure at very high Marangoni number has also been established. Unfortunately, the assumption of a perfectly cylindrical free surface, although it appears to reflect quite well the 0-g condition, has imposed a severe restriction to any further study in 1-g condition. In the present paper, a more realistic physical model, which takes into account the deformability of the free surface, has been proposed. Simulations were performed under unsteady regime where the flow and thermal fields, subjected to a realistic heating process, develop from the known initial state. The time-development of zones operating under 1-g and μ-g (i.e. 10^{-4}g) with $NaNO_3$ and Silicon will be presented and discussed.

Mathematical formulation

a) Governing equations

We consider a cylindrical half-zone of a molten liquid which is held, under surface tension effect, between a pair of coaxial, parallel disks of radius R_0 and separated from each other by the distance H (Figure 1a). The disks are stationary and isothermal at uniform temperatures $t_1 = f(\tau)$ and $t_2 = t_M$, where $f(\tau)$ is an a priori known function of time specifying the heating process and t_M is the melting temperature of the material considered. For a proper mathematical formulation of the problem, the fluid is assumed to be incompressible with constant properties evaluated at t_M, except for the density appearing in the buoyancy forces where the Boussinesq's approximation prevails. The flow and thermal field are both axisymmetric. The compression work as well as the viscous dissipation in the energy equation are considered to be negligible. Under these conditions, the dimensionless governing equations written in the cylindrical coordinates system are as follows:

$$\frac{\partial V_R}{\partial R} + \frac{\partial V_Z}{\partial Z} + \frac{V_R}{R} = 0 \tag{1}$$

$$\frac{DV_R}{D\tau*} = -\frac{\partial P}{\partial R} + \frac{1}{Re_{th}}\left(\nabla^2 V_R - \frac{V_R}{R^2}\right) \tag{2}$$

$$\frac{DV_Z}{D\tau^*} = -\frac{\partial P}{\partial Z} + \frac{1}{Re_{th}}\nabla^2 V_Z - \frac{Bd}{Re_{th}}T \tag{3}$$

$$\frac{DT}{D\tau^*} = \frac{1}{Ma}\nabla^2 T \tag{4}$$

where

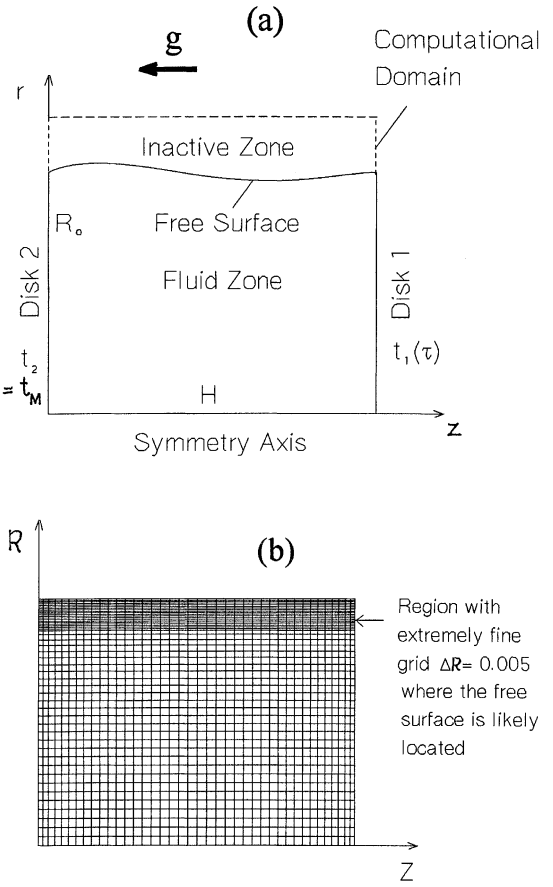

Figure 1.
(a) Geometry of the problem studied, and (b) the grid used for computation.

$$\frac{D}{D\tau^*} = \frac{\partial}{\partial\tau^*} + V_R\frac{\partial}{\partial R} + V_Z\frac{\partial}{\partial Z} \tag{5}$$

$$\nabla^2 = \frac{\partial^2}{\partial R^2} + \frac{1}{R}\frac{\partial}{\partial R} + \frac{\partial^2}{\partial Z^2} \tag{6}$$

In order to obtain the above equations, the following quantities $H, |\partial\ \sigma/\ \partial\ T\ |\ \Delta\ T/\mu)$, $(H\ \mu/\ |\ \partial\ \sigma/\partial\ T\ |\ \Delta\ T), \rho(|\partial\sigma/\partial T|\Delta T/\mu)^2$, and $\Delta T = tt_1 - t_2$ have been adopted as the reference length, velocity, time, pressure and temperature difference respectively (tt_1 is the disk no. 1 temperature corresponding to each of the step cases considered – see Figure 2). A dimensionless variable is obtained by normalizing the quantity considered

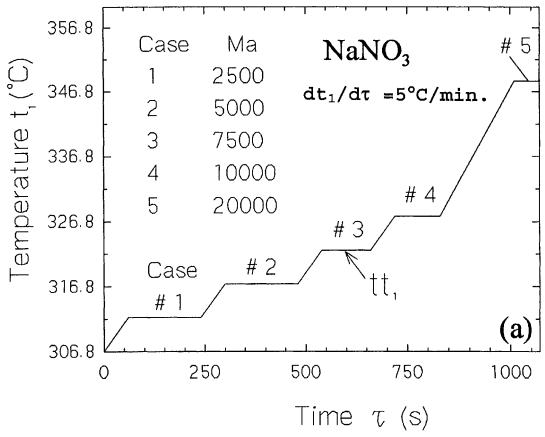

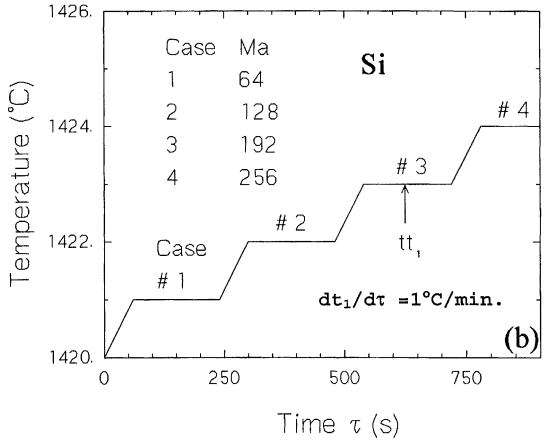

Figure 2. Comparison with experimental data for: (a) $NaNO_3$, steady-state case and (b) Silicone oil float zones, unsteady case.

with respect to the corresponding reference quantity. The dimensionless temperature is defined as:

$$T = \frac{(t - t_2)}{\Delta T} \tag{7}$$

b) Boundary and initial conditions

In order to completely define the problem under consideration, one must introduce the following hydrodynamic and thermal boundary conditions (Equations 8-11) as well as the initial conditions (Equation 12):

$$i.\quad \text{at } Z = 0 \quad : \quad V_R = V_Z = 0\,, \quad T = 0 \tag{8}$$

$$ii.\quad \text{at } Z = 1 \quad : \quad V_R = V_Z = 0\,, \quad T = f(\tau^*) \tag{9}$$

$$iii.\quad \text{at } R = 0 \quad : \quad V_R = 0\,, \quad \frac{\partial V_Z}{\partial R} = \frac{\partial T}{\partial R} = 0 \tag{10}$$

$$iv.\quad \text{at } R = \frac{R_0}{H} = A \quad : \quad V_R - \frac{\partial F}{\partial Z} V_Z = 0 \tag{11a}$$

$$2\frac{\partial F}{\partial Z}\left(\frac{\partial V_R}{\partial R} - \frac{\partial V_Z}{\partial R}\right) + \frac{\partial V_Z}{\partial R} + \frac{\partial V_R}{\partial Z} = -\left(\frac{\partial F}{\partial Z}\frac{\partial T}{\partial R} + \frac{\partial T}{\partial Z}\right) \tag{11b}$$

$$CaRe_{th}P - BsZ = \frac{1}{F} - \frac{\partial^2 F}{\partial Z^2} \tag{11c}$$

$$\frac{\partial T}{\partial R} - \frac{\partial F}{\partial Z}\frac{\partial T}{\partial Z} = 0 \tag{11d}$$

where F = F(Z) is the local radius of the deformed surface.

$$\nu.\quad \text{at } \tau^* = 0 \quad : \quad V_R = V_Z = 0\,, \quad T = 0 \tag{12}$$

Equations (8, 9) express the non-slip and non-penetration conditions usually encountered on solid surfaces. On the disk no. 2, the fluid temperature is constant and identical to t_M; while the disk no. 1 temperature is variable with time according to Figure 2. Equation (10) represents the symmetry conditions for both the velocity and temperature fields with respect to the centerline. The equations 11a, b, c and d specify the boundary conditions on the free surface. Thus, we assume zero mass flux across that surface (Equation 11a) as well as the equilibrium condition of tangential and normal stresses (Equations 11b and 11c). Also, the free surface is considered as thermally adiabatic with respect to the surrounding environment (Equation 11d). This condition appears to be quite appropriate to approximate the real operating conditions (see for example, Preisser *et al.,* 1983). Note that the equations 11(a-d) have been obtained based on the assumptions Ca <<1 and $(\partial F / \partial Z)^2$ <<1. The former holds true for the cases studied here where the maximum value of Ca is about 0.009; while the latter is valid only for weakly deformed free surface. These conditions have been thoroughly verified by a complete study of order of different terms in Equations 11b,c (Bazzi, 1999). It is interesting to mention here that the assumption $(\partial F / \partial Z)^2$ <<1 has also been used by many researchers, see for example Lai (1984) and Duranceau and Brown (1986), in similar studies on float zones. The complementary details regarding the mathematical obtention of the equations 11 (a-d) are given in the Appendix.

With regard to the initial conditions, Equation (12) specifies the rest state where the fluid temperature is uniform and equal to the melting temperature at the beginning of the heating process. (i.e. at $\tau = \tau^* = 0$).

We finally note that, from the governing equations (1-4) and their boundary and initial conditions (8-12), the problem under study may be characterized by a set of seven dimensionless parameters, namely the aspect ratio A, the thermocapillary Reynolds number Re_{th}, the Prandtl number Pr, Marangoni number Ma, the dynamic Bond number Bd, the static Bond number Bs and the capillary number Ca. Their definition is given in the Nomenclature.

c) Boundary conditions for the function F(Z)

The instantaneous position of the free surface is obtained by solving the equation (11c) subject to the following boundary conditions:

$$i. \quad \text{at} \quad Z = 0 \quad : \quad \frac{\partial F}{\partial Z} = -\tan\gamma \tag{13a}$$

$$ii. \quad \text{at} \quad Z = 1 \quad : \quad \frac{\partial F}{\partial Z} = \tan\gamma \tag{13b}$$

$$iii. \quad F(0) = F(1) = A \quad , \quad \text{and} \tag{13c}$$

$$iv. \quad \int_0^1 [F(Z)]^2 \, dZ = A^2 \tag{13d}$$

The equations 13(a-c) simply express the conditions of adherence of the liquid zone on both end disks (γ represents in fact the contact angle); while the equation (13d) stipulates that the volume of the liquid zone is constant and equal to the corresponding volume of a non-deformed cylindrical liquid zone.

Numerical method

The system of governing equations (1-4), subject to the boundary and initial conditions (8-12), constitutes a highly non-linear and coupled system. They must be solved appropriately in order to determine the flow structure and the thermal field as well as their time-evolution. It should be noted that the position of the free surface is unknown a priori and must be computed as part of the solution. In the present study, the modified-SIMPLE method incorporated within the computer code named Micro-COMPACT has been adopted for the task demanded. Details regarding this method have been extensively documented in Patankar (1980, 1996).

a) Determination of the position of the free surface

The instantaneous (i.e. at every time-step) position of the zone free surface must be appropriately determined by solving the equation (11c) expressing the normal-stress balance which is subjected to the boundary conditions (13a-d). The following procedure has been adopted in this study:

(1) first, the static shape of the free surface, i.e. the one corresponding to the isothermal liquid zone $Re_{th} = 0$, is determined by solving the equation (A.21) subject to the same boundary conditions (13a-d) by employing a standard Runge-Kutta (order four) algorithm – see Burden *et al.* (1981). The shape of the free surface obtained is then used as initial condition in the next step.

(2) Since we wish to calculate the position of the free surface at every time-step, a special procedure has been proposed and incorporated within the Micro-COMPACT code. This procedure consists of considering the function F(Z) – a one-dimensional variable – as a dependent variable. The equation (11c) can be then cast into a generalized form which is treatable by the code. Some special provisions and modifications were implemented to take into account the one-dimensional nature of F(Z). The following steps resume the procedure:

- starting with the static shape obtained from the previous step,
- solve the discretized equation of the equation (11c) by using a modified-SIMPLE algorithm,
- correct the value of the function F(Z) according to the condition (13d),
- continue the calculation until convergence i.e. the condition (13d) is fully satisfied within an acceptable error.

Note that the above steps must be performed at every time-step prior to the calculation of the flow and the thermal field. The complete details regarding the procedure of the determination of the free surface may be found in Bazzi (1999).

b) Treatment of the free surface / the calculation procedure

The presence of the free surface requires a special attention here, particularly for a "regular-fixed-grid" method as the one used in this study. A successful special procedure has been proposed. According to this procedure, the calculation domain which is extended beyond the free surface, has been split into two different zones: the fluid zone and the inactive zone (Figure 1b). In the fluid zone, the resolution of the governing equations proceeds following the modified-SIMPLE algorithm, and this, employing appropriate fluid properties. In the inactive zone, we have used the "very large-source" approach, as proposed by Patankar (1980, 1996), in order to be able to impose the desired radial velocity (Equation 11a), the temperature gradient (Equation 11d), and the axial velocity gradients (Equation 11b) on the free surface. The instantaneous position of that free surface is determined by appropriately solving the

Equation (11c) expressing the normal stresses equilibrium, assuming the static shape i.e. the one corresponding to Equation (11c) with however Ca Re P = 0, at $\tau^* = 0$. The calculation procedure for every time step may be summarized as follows:

- compute the position of the free surface by solving Equation (11c) subject to the appropriate boundary conditions according to the procedure detailed in "(a)";
- assign appropriate values for properties and coefficients to "fluid" and "inactive" volumes;
- solve the system of discretized equations of Equations (1-4) following the modified-SIMPLE method, to obtain the new velocities and temperature fields;
- correct the axial velocity and the temperature along the free surface, by using the discretized form of the Equations (11b) and (11d). Note that the discretized equations have been obtained by employing the standard central-differencing technique.

c) Choice of the grid

The choice of the grid is particularly crucial due to the presence of the curved free surface where the calculation of the temperature and velocity gradients must be as precise as possible. Since a fixed grid is used and the free surface has to be approximated by a set of interconnected straight segments, the grid should then be very fine in the region near that free surface. It should be noted that the grid was constructed based on the knowledge of the position of the free surface as obtained in the static case. Several non-uniform grids were thoroughly tested and compared, based on the flow and thermal structure and, in particular, on the temperature and axial velocity profiles on the free surface. The non-uniform 42×50 grid (42 and 50 nodes, respectively, along the axial and radial directions) has been adopted for the task demanded. The grid offers highly packed grid points along both disks and, especially, along the free surface where radial increment ΔR has been drastically reduced to 0.005 (Figure 1b). The grid requires a reasonable amount of efforts in term of the numerical computation and offers a quite acceptable accuracy of the results. Thus, the results on the velocity and temperature as given by the 42×50, 48×44 and 52×40 non-uniform grids exhibit no significant differences (see Bazzi, 1999).

d) Choice of $\Delta\tau$ and convergence criteria

For all the cases considered in this study, the time step $\Delta\tau$ been fixed to 1 S for low Marangoni numbers, while for Ma > 7,500, $\Delta\tau$ has been reduced to 1 / 8 S. These values were found to be quite appropriate for the fluids considered, $NaNO_3$ and Silicon, and the heating-up schemes adopted.

As convergence criteria, we mainly used the residual mass resulting from the integration of the continuity equation (Equation 1) over the finite control

volumes. For every time step, the converged solutions which required, in the average, from 20 to 30 "inner" iterations (the "inner" iterations refer to the iterations performed on the set of the discretized equations within one single time-step), were usually obtained with a very low value of this residual mass. The maximum residual mass has not exceeded, in any case, 0.001 per cent. The relaxation factors were fixed to 0.4 for velocity components and 0.6 for temperature; no numerical instabilities or convergence problems were observed, so far, during all of the simulations performed.

e) Validation of the mathematical model

The computer code has been thoroughly validated by comparing numerical results as obtained for a $NaNO_3$ half-zone under steady-state condition to the corresponding experimental measures and observations by Preisser *et al.* (1983). Figure 3a shows such a comparison of the fluid circulation on the free surface. The agreement can be qualified as quite acceptable, in conjunction with the uncertainty that may be expected in the determination of the local velocity on the free surface by mean of the optical-particles-tracing technique. A good concordance has also been found between numerical results and

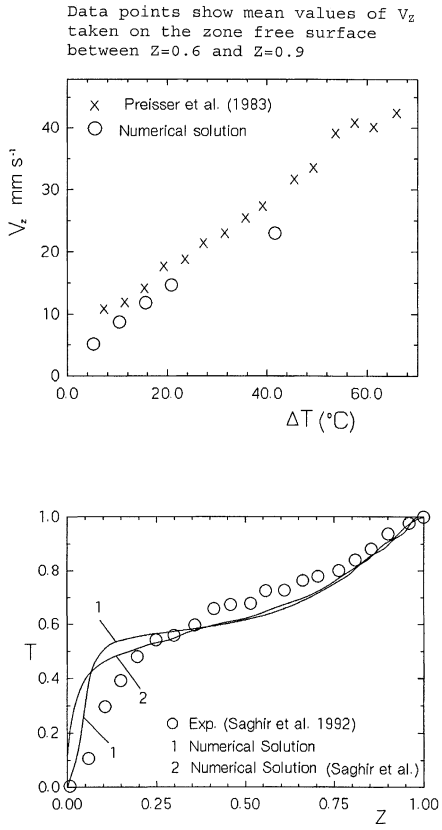

Figure 3.
Time-evolution of the heated disk temperature for: (a) $NaNO_3$ and (b) Si.

experimental observations by Preisser *et al.* (1983) regarding the flow structure and the thermal field obtained for the case Ma = 4,800 (see Bazzi, 1999). In the second serie of validation tests, the computer code has been used to study the transient behaviours of a Silicon oil half-zone under 1-g condition where the disks temperatures are function of time following the same trends as experimentally imposed by Saghir *et al.* (1992). A good agreement has been found with data from Saghir *et al.* (1992) regarding the structure of the flow and thermal fields for several "pseudo-steady-states" (i.e. corresponding to a constant ΔT between disks). Figure 3b shows a comparison between our results and the corresponding experimental data and numerical results by Saghir *et al.* (1992) as obtained for a typical case (Ma = 617.5, Re_{th} = 3.14, Pr = 196.5, Bs = 7.17, and Bd = 2.66). Compete details regarding the choice of the grid and the validation tests may be found in Bazzi (1999).

Results and discussion

After the mathematical model as well as the chosen numerical method have been satisfactorily validated, the computer code has been used to study the transient behaviour of the hydrodynamic and thermal fields, with emphasis on the structure of the flow at high Marangoni number. Results will be presented for two different fluids, namely $NaNO_3$ (Pr = 8.9) and Silicon (Pr = 0.016) for both 1-g and μ-g conditions. Note that the physical properties of the molten liquid $NaNO_3$ and Silicon have been taken from Preisser *et al.* (1983) and Saghir (1987).

a) Time-evolution of the hydrodynamic and thermal fields for $NaNO_3$ float zones

Figure 2a shows the transient evolution of the hot disk (i.e. disk no. 1) temperature as imposed for the simulations performed on $NaNO_3$. Note that the slope $dt_1 / d\tau$ was fixed to 5°C/ minute, value which appears to be reasonable according to Schwabe and Sharmann (1983). Figures 4 and 5 show respectively, the time-evolution of the axial velocity and temperature profiles along the free surface for the typical cases (Ma = 5,000, Re_{th} = 562, Ca = 0.0048) and (Ma = 10,000, Re_{th} = 1124, Ca = 0.0096). The aspect ratio A has been fixed to 0.732, and the static and dynamic Bond number were, respectively, 2.66 and 2.16 under 1-g condition. Note that these values of the governing parameters correspond to a zone with dimensions R_0 = 3mm and H = 4.1mm.

It is observed that, in general, the axial velocity and temperature gradients are much more pronounced in the vicinity of the disks while over a relatively large area of the central region on the free surface, the fluid temperature and circulation are almost uniform. We also notice the similar shape of axial velocity and temperature profiles during the heating duration. With regard to the comparison 1-g versus μ-g conditions, one may notice a striking difference on the V_Z profiles near the cold disk. We can observe that under 1-g condition, there exists a narrow region where V_Z becomes positive, indicating obviously that fluid is directed towards the hot disk (i.e. in the opposite direction with

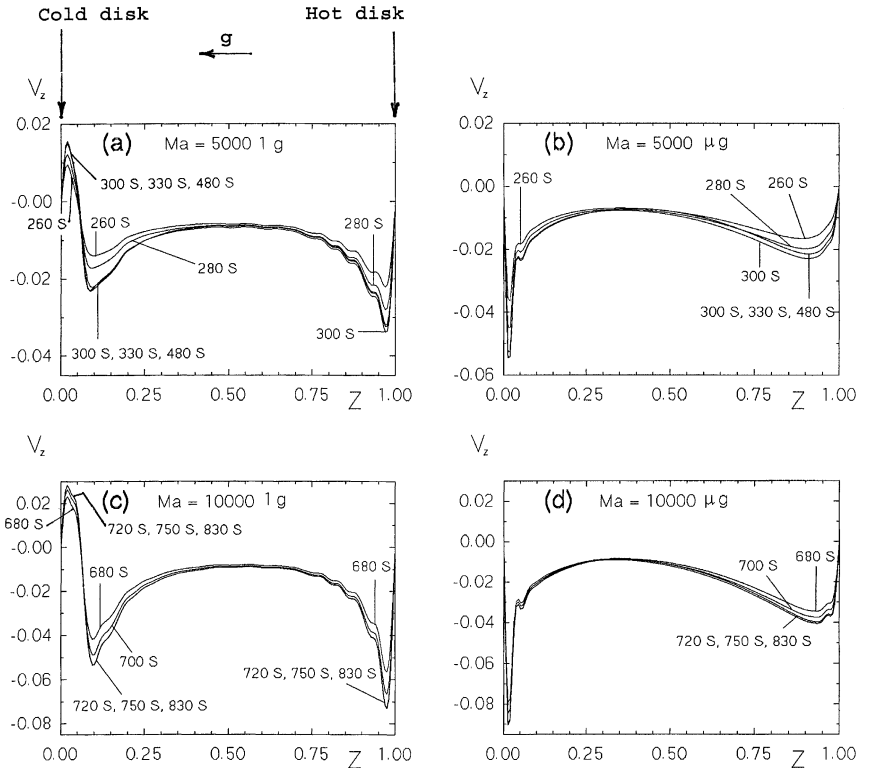

Figure 4.
Time-evolution of the axial velocity profile on the free surface for $NaNO_3$ float zone (Ma = 5,000 and 10,000, A = 0.732).

respect to the thermocapillary flow). Such behaviour, which has not been observed under μ-g condition, may be explained later by scrutinizing the structure of the flow field (Figures 6 and 7). For instance from Figure 5, it is clearly observed that, for a given Marangoni number, the fluid temperature appears to be much higher under μ-g condition than in normal gravity condition. Such behaviour results from the fact that under 1-g condition, natural convection effects exist and they, with respect to the geometrical configuration studied here, oppose the thermocapillary effects. This combination results in a reduction of the thermocapillary flow, and hence, one may expect that the heat transfer in the fluid zone is improved under μ-g condition. It is also observed that in the vicinity of the cold disk, the axial temperature gradient is greatly reduced in zones operating under 1-g condition.

The above interesting hydrodynamic and thermal behaviours related to the free surface may be better understood by scrutinizing Figures 6, 7 and 8 which show, respectively, the time-evolution of the flow structure and isotherms as obtained for the same cases considered earlier. We can observe that, in general, the circulation of the fluid is more intense along the free surface and, also, the center of the thermocapillary recirculation zone is located near that free surface. These characteristics are well known to any thermocapillary flow such as the one under study here. For relatively low and moderate Marangoni number

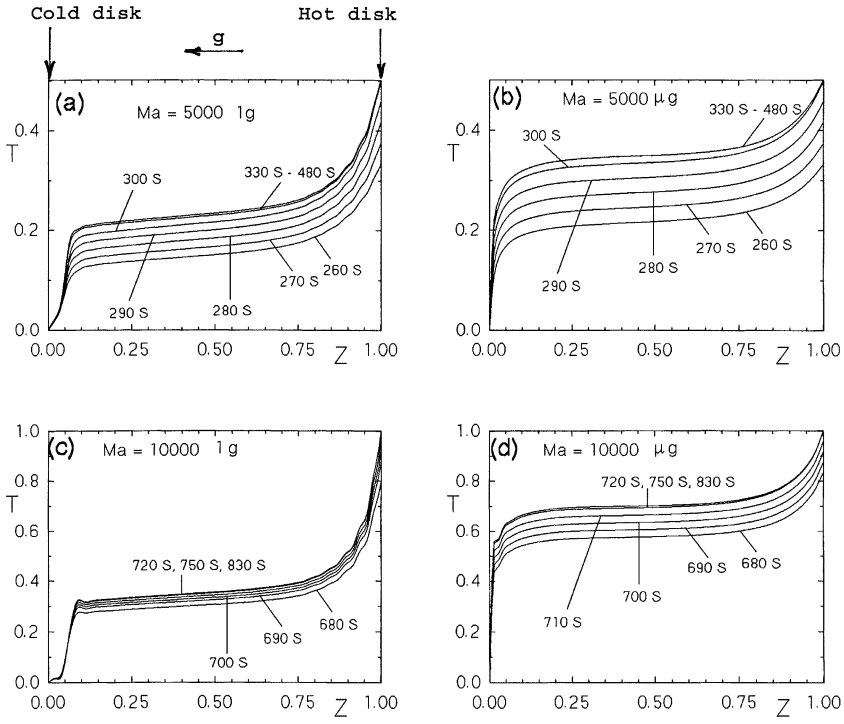

Figure 5.
Time-evolution of the temperature profile on the free surface for $NaNO_3$ float zone (Ma = 5,000 and 10,000, A = 0.732).

under 1-g and μ-g, say Ma $\leq$ 5,000, the usual unicellular flow structure has been found with the recirculation zone located beside the heated disk. Such behaviour has also been observed for high Marangoni number, say Ma = 10,000, under μ-g condition only (Figure 7). For the case Ma = 10,000 under 1-g, however, the bicellular flow structure may be expected, due to the fact that the thermocapillary flow becomes stronger near the cold disk. Since the radial temperature gradient within the fluid is more important under high Marangoni number, the natural convection effects on the return flow become, consequently, more important. That explains the presence of a stronger recirculation of the fluid near the cold disk. For cases operating under 1-g, it is rather interesting to notice the presence of a tiny recirculation zone located in the vicinity of the cold disk (Figues 6 and 7). Such recirculation zone which causes positive axial velocity on the free surface (Figure 4), is believed to be due essentially to the curved shape of the free surface. No such behaviour has been observed for cases under μ-g condition where the free surface remains nearly cylindrical. In fact, for the μ-g cases considered, numerical results have shown that the maximum deformation of the free surface corresponding to 10^{-4}g does not exceed 0.08 per cent of the zone nominal radius. Hence, the assumption of a perfectly cylindrical free surface as often considered by many researchers in studying zones operating in μ-g conditions (see for example, Rupp *et al.,* 1989) appears to be quite acceptable.

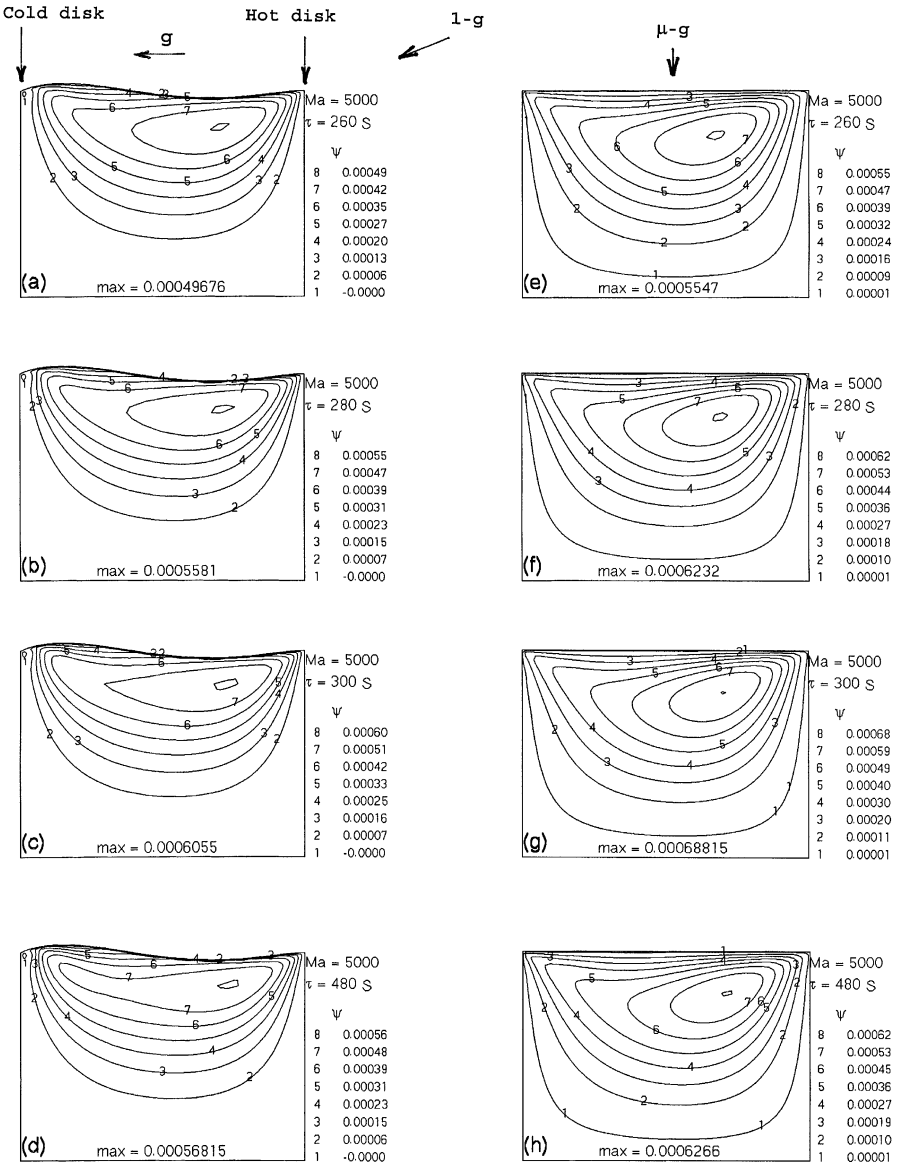

Figure 6.
Time-evolution of the flow field in $NaNO_3$ float zone Ma = 5,000, A = 0.732 under 1-g (a-d) and μ-g (e-h) conditions

With regard to the transient behaviour of the flow and thermal fields, it is observed that, although they exhibit only a minor changes in their structures with time, the maximum value of the stream function, Ψ_{max} – which indicates the intensity of the thermocapillary flow – increases steadily with time during the heating process. One may notice, for a given case, the existence of a maximum value of Ψ_{max} observed shortly after the temperature of the heated disk has reached its constant value. Afterwards Ψ_{max} decreases slightly to reach a certain asymptotic value which corresponds to a fixed (i.e. constant) temperature

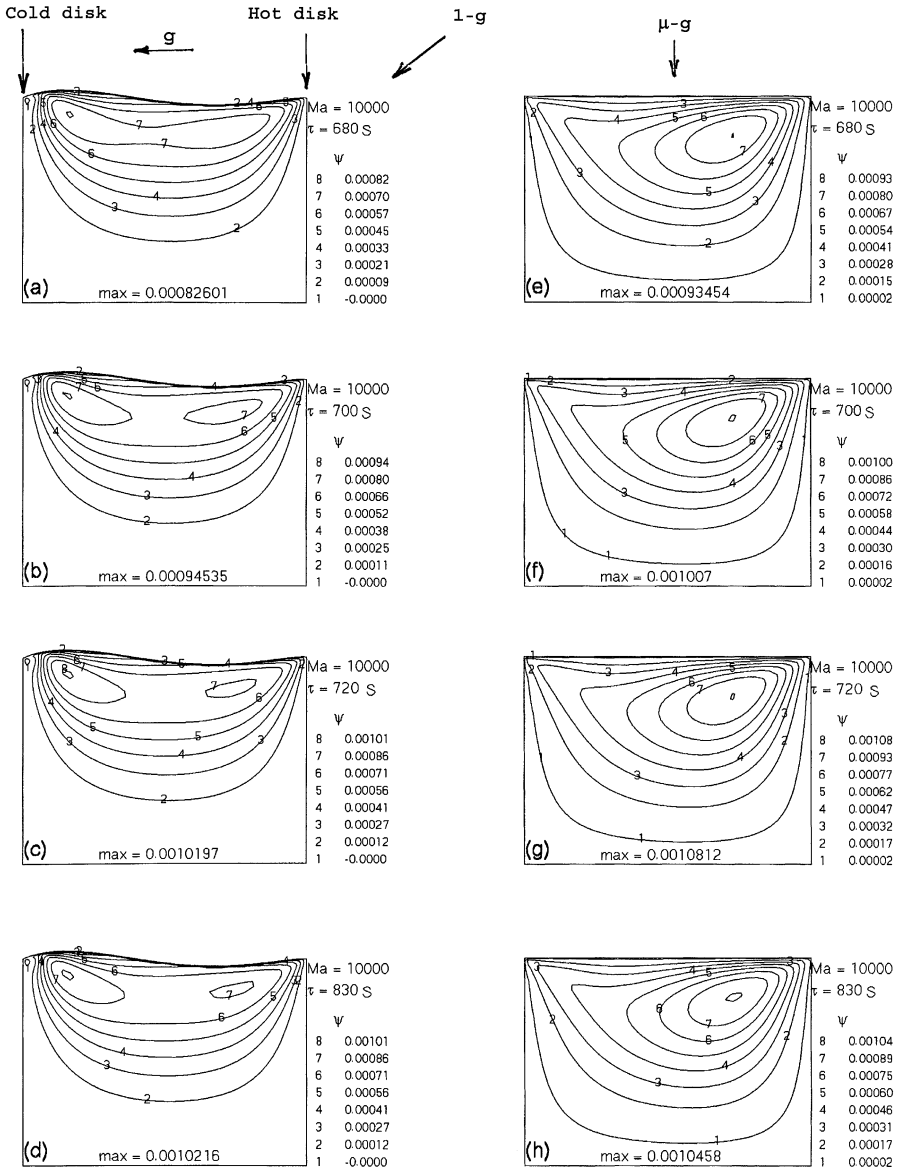

Figure 7.
Time-evolution of the flow field in $NaNO_3$ float zone Ma = 10,000, A = 0.732 under 1-g (a-d) and μ-g (e-h) conditions

difference between the disks. This behaviour, also observed by Nguyen *et al.* (1995a) under μ-g condition, may be attributed to the stabilization of the thermocapillary flow itself, which can be explained as follows. At the end of the heating process and shortly after the heated disk temperature reaches its constant value (corresponding to the end of each of the steps), the thermocapillary flow has gained a considerably strong intensity. Unless we continue to impose an increasing ΔT between the disks, this strong

thermocapillary flow will tend to uniformize the temperature field. As a consequence, the temperature gradient on the free surface will decrease slightly and so, in turn, does the intensity of the thermocapillary flow. Another point of particular interest resides in the fact that the shape of the free surface remains essentially the same during the heating process and it is almost identical to the one corresponding to the static condition. Such a result appears to be quite realistic since for low capillary number fluid such as the one studied here, it is well known that the shape of the free surface is mainly governed by gravity and surface tension effect. In fact for the sake of generality as well as for future study on the oscillatory flow, we have conserved the term "Ca Re_{th} P" in Equation 11c, but its omission will not produce any significant effect on the shape of the free surface. It is very interesting to note that the assumption of a low capillary number fluid – i.e. neglecting the term "Ca Re_{th} P" – has also been considered by many researchers (see for example Kozhoukharova and Slavchev, 1986).

Regarding the transient behaviour of the thermal field, for Ma = 5,000 in particular (Figure 8), we can observe that at the beginning of the heating process, hot fluid is mainly confined near the heated disk. With further increase in time, the hot front invades progressively the fluid zone. We notice an appreciable increase of the temperature gradient with time, in particular near the hot disk. One may also observe the distorted isotherms along the free surface. The distortion results from the thermocapillary effects. Such distortion is clearly more pronounced under μ-g condition indicating a stronger intensity of the thermocapillary flow, as discussed previously.

Finally, it is observed that the intensity of the thermocapillary flow also increases considerably with the increase of the Marangoni number. Such obvious behaviour may be explained by the fact that with an increase of Ma (and hence, an increase of ΔT between the disks), the driving temperature gradient will increase and consequently, the resulting thermocapillary flow will become more important. Table I shows such influence of the Marangoni number Ma on the values of Ψ_{max} as well as on the fluid circulation V_Z (at Z = 0.6) corresponding to the asymptotic thermal boundary conditions for both the μ-g and 1-g environments (note that all the values of Ψ_{max} in Table I have been converted using the same base corresponding to Ma = 10,000). As discussed previously, the thermocapillary flow is improved under μ-g condition. This behaviour is clearly observed from Table I.

b) Time-evolution of the hydrodynamic and thermal fields for Silicon float zones

We were particularly interested to study the transient behaviours of a Si (Pr = 0.016) float zone because this material is widely used in semiconductors fabrication. Most of our numerical simulations were carried out for μ-g condition. A parametric study has been performed in order to investigate the effects of both the Marangoni number Ma and aspect ratio A. Figure 2b shows the time-evolution of the disk no. 1 temperature as imposed for the simulations performed on Si. Note that the slope $dt_1/d\tau$ was fixed to 1°C/minute and the continuous heating process is started from the rest state with uniform

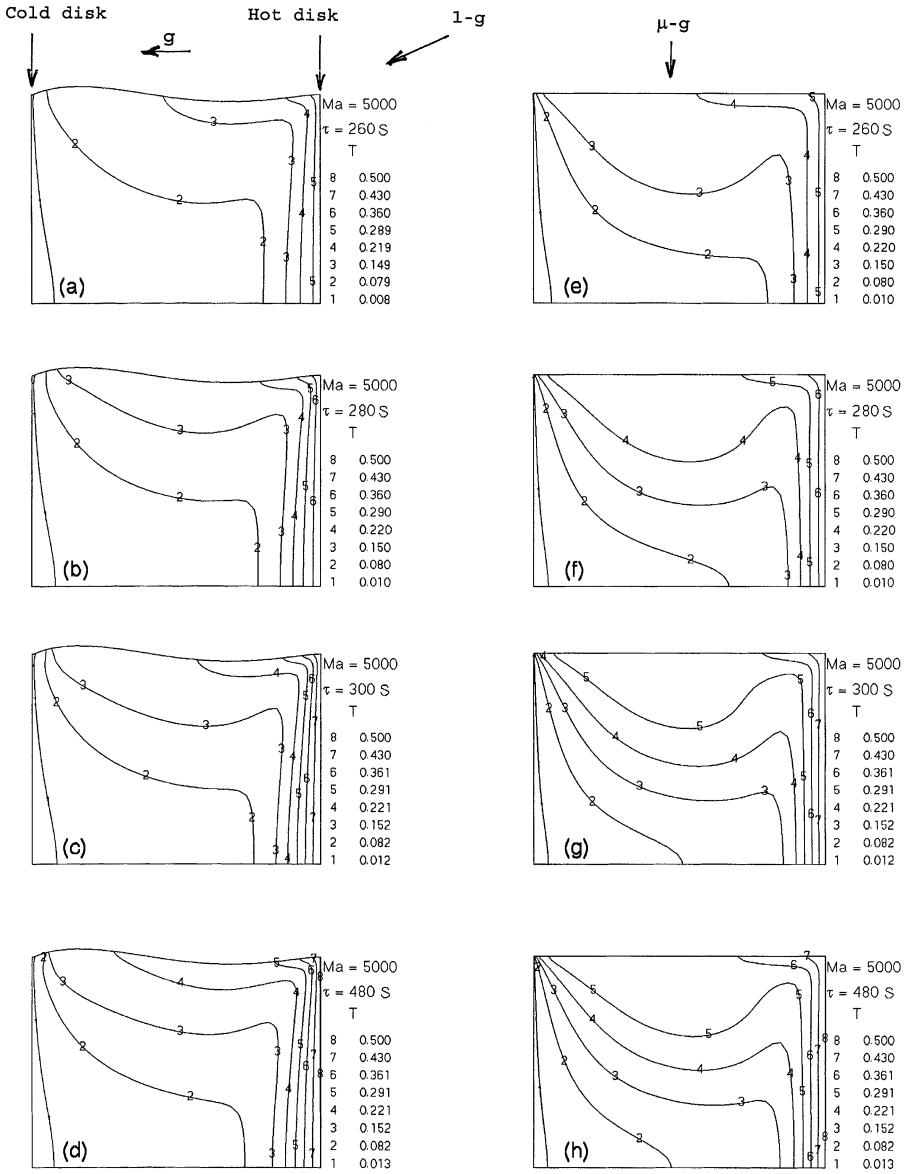

Figure 8.
Time-evolution of the isotherms structure in $NaNO_3$ float zone Ma = 5,000, A = 0.732 under 1-g (a-d) and μ-g (e-h) conditions

Ma	2,500	5,000	7,500	10,000
V_Z (mm/s) Z = 0.6 (1-g)	2.04	2.71	3.35	3.85
V_Z (mm/s) Z = 0.6 (μ-g)	3.06	4.25	5.41	6.8
Ψ_{max} (1-g)	3.858×10^{-4}	5.68×10^{-4}	7.823×10^{-4}	1.02×10^{-3}
Ψ_{max} (μ-g)	4.203×10^{-4}	6.26×10^{-4}	8.280×10^{-4}	1.04×10^{-3}

Table I.
Effects of Ma on Ψ_{max} and the fluid circulation on the free surface for $NaNO_3$ float zone

temperature equal to the melting temperature t_M of Silicon. Figure 9 shows in particular the transient evolution of the fluid temperature and the axial velocity on the free surface as obtained for the case Ma = 64, Re_{th} = 4,000 and A = 0.7. We can notice immediately a striking difference regarding the behaviours of a Si zone while comparing to that of a $NaNO_3$ zone. It is observed, at first, that the temperature profiles are almost linear along the free surface indicating clearly the dominant effect of the conduction, as we know that Si has a high thermal conductivity. Also, the temperature gradient is generally important near the disks and increases with time. Such increase has been found to be remarkable near the cold disk, which explains the movement of the point of the maximum axial velocity towards that end. Near the hot disk, however, one can notice the diminution of the temperature gradient between τ = 60 S and τ = 90 S, which causes consequently a decrease in the fluid circulation velocity. Such behaviour may be attributed to the stabilization of the thermal field, as discussed previously. For the case shown, the stabilization time (i.e. the elapsed time between the start-time of the heating and the moment where the flow is declared fully-developed) may be estimated to be $\approx$ 90 seconds during which, the maximum value of V_Z has increased almost by the factor of three. We also

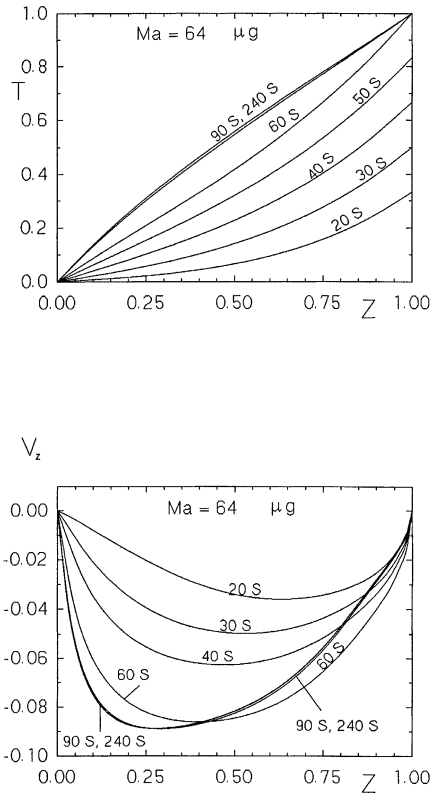

Figure 9.
Time-evolution of the temperature and axial velocity profiles on the free surface for a Silicon float zone under μ-g condition (Ma = 64, A = 0.7)

observe that, in opposition to a $NaNO_3$ float zone (Figure 4), the thermocapillary flow is pronounced all along the free surface with a single point of the maximum V_Z observed, for the case considered, near the cold disk. Figure 10 shows, respectively, the structure of streamlines and isotherms as obtained for the case under consideration at different times during the heating process. One may clearly noticed the nearly cylindrical free surface since, as noted previously, the radial deformation of that free surface is negligible under μ-g condition. It is very interesting to observe, at first, that the shape of the

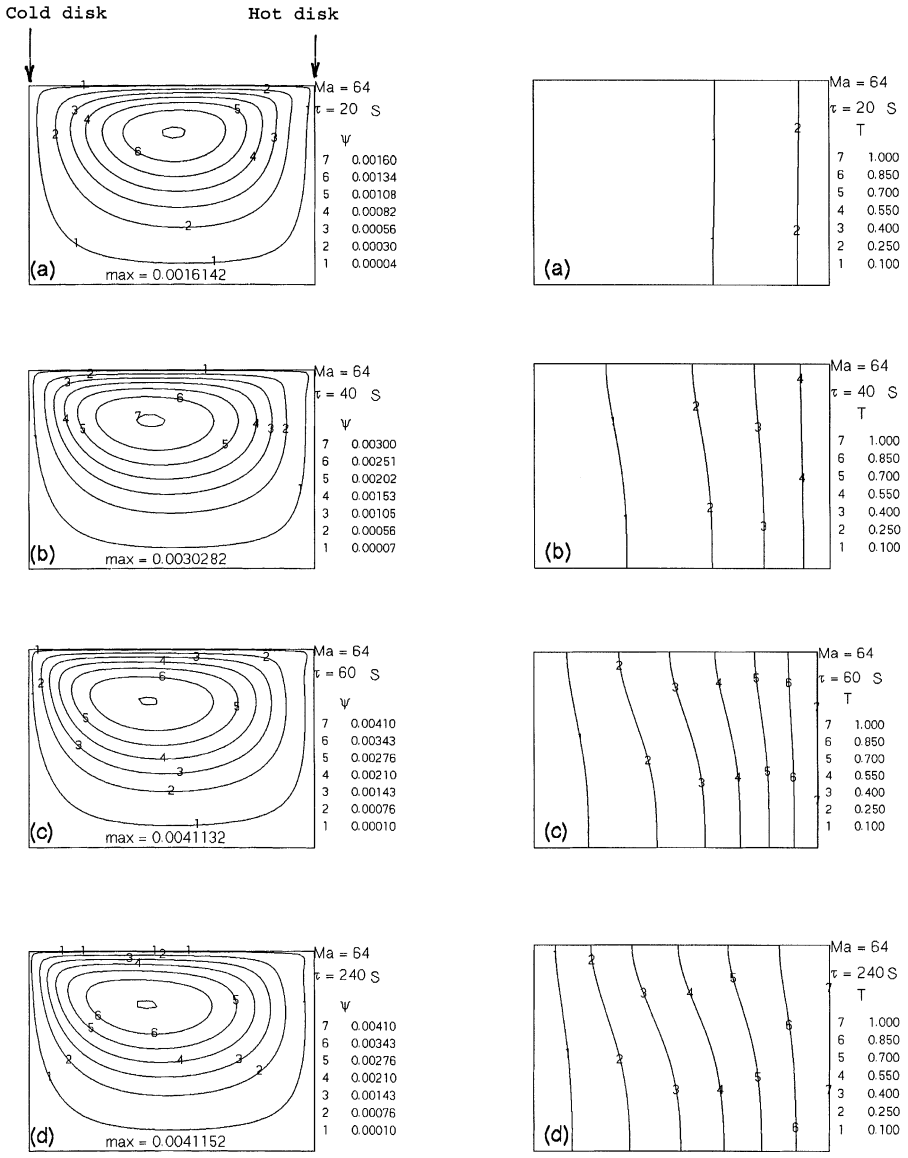

Figure 10.
Time-evolution of the flow field and isotherms in a Silicon float zone under μ-g condition (Ma = 64, A = 0.7)

streamlines remains almost the same with time. The flow structure consists of an usual unicellular pattern with strong circulation of fluid along its free surface. The value of Ψ_{max} is respectively, 1.61×10^{-3}, 3.03×10^{-3}, 4.11×10^{-3} and 4.11×10^{-3} for τ = 20, 40, 60 and 240 S. Hence, the structure obtained at τ = 60 S may be regarded as the one corresponding to the asymptotic state of the flow. With regard to the thermal field, one can see that its structure consists generally of parallel straight lines. Only at the end of the heating process where Ψ_{max} becomes considerable, slightly curved isotherms can be clearly noticed. Such behaviour may be explained by the fact that Si is a relatively high thermal conductivity and low viscosity material for which, the thermal structure would be governed almost entirely by the imposed boundary conditions and it is not significantly affected by the flow field. The above hydrodynamic and thermal behaviours have also been found for other values of Ma and A tested in this study (Bazzi, 1999).

Similar behaviours regarding the influence of the Marangoni number have been found for a Si float zone. For example, the value of Ψ_{max} corresponding to a "pseudo-steady-state" has increased from 4.11×10^{-3} to 6.47×10^{-3} to 8.18×10^{-3} and to 9.55×10^{-3} for Ma augmenting from 64 to 128 to 192, and to 256. On the other hand, the corresponding values of V_{Zmax} on the free surface are, respectively, 0.0877, 0.1455, 0.1929 and 0.2366.

With respect to the influence of the aspect ratio A, it has been observed that Ψ_{max} also increases considerably with an augmentation of A. Thus, for the case Ma = 123, Ψ_{max} is respectively 0.0038, 0.0052, 0.0065 and 0.0098 for A = 0.5, 0.6, 0.7 and 1.0. However, V_{Zmax} does not vary significantly with A. In fact, it decreases slightly with an increase of A. The corresponding values of V_{Zmax} are 0.1472, 0.1469, 0.1455 and 0.1424. Such behaviours may be explained by the fact that increasing the aspect ratio A (defined as R_0 / H) is equivalent, within the context of this study where H has been chosen as the reference length, to an increase of R_0 or of the volume of the fluid itself under the free surface. Hence, one can expect that the thermocapillary flow would be improved. The above apparent contradictory behaviour regarding the decrease of V_{Zmax} with A is believed to be due to the slight movement of the center of the recirculation zone away from the free surface.

Table II resumes finally the effects of both the parameters Ma and A on the asymptotic values of Ψ_{max} and the fluid circulation V_{Zmax} under μ-g condition.

Table II.
Effects of parameters Ma and A on Ψ_{max} and V_{Zmax} for silicon float zone

		A = 0.7		
Ma	64	128	192	256
Ψ_{max}	4.11×10^{-3}	6.47×10^{-3}	8.18×10^{-3}	$9.55\times10^{-3)}$
V_{Zmax}(mm/s)	45.30	74.31	98.53	120.84
		Ma = 128		
A	0.5	0.6	0.7	1
Ψ_{max}	$3.88\times10)^{-3}$	5.20×10^{-3}	6.47×10^{-3}	9.83×10^{-3}
V_{Zmax}(mm/s)	75.18	75.02	74.31	72.73

Note that the values of Ψ_{max} and V_{Zmax} in Table II have been all converted using the same base corresponding to the case Ma = 64, since the reference velocity is function of the temperature difference between the disks.

Conclusion

In this work, a successfully validated numerical model which takes into account the deformability of the free surface has been proposed to study the transient behaviour of $NaNO_3$ and Silicon float zones operating under μ-g and 1-g environments. From the numerical results obtained, the following conclusions seem to be pertinent:

- in general, the temperature and velocity gradients are more pronounced near the disks and a stronger fluid circulation is observed along the free surface;
- these gradients as well as the intensity of the thermocapillary flow increase steadily with time during the heating process to reach a certain maximum state and decrease slightly afterwards to an asymptotic state as the temperature difference between the disks becomes constant;
- the intensity of the asymptotic thermocapillary flow increases considerably with the increase of the Marangoni number. This intensity also increases with an augmentation of the aspect ratio;
- the thermocapillary flow and the heat transfer have been found to be improved under μ-g condition;
- for the cases studied, the dynamical shape of the free surface has been found to be nearly identical to the one corresponding to the static condition;
- for $NaNO_3$ float zones with low to moderate Marangoni numbers under 1-g condition as well as for all the cases operating in μ-g environment, the unicellular flow structure has been found with the recirculation center located near the heated disk. On the other hand, the bicellular flow structure may be observed for a case with high Marangoni number under 1-g condition;
- for a Silicon float zone under μ-g condition, only a unicellular flow structure has been observed with the center of the recirculation zone located near the cold disk.

References

Bazzi, H. (1999), "Étude numérique de l'écoulement transitoire dans une zone flottante – La transition axisymétrique/oscillatoire", "Numerical study of the axisymmetric/oscillatory transition in a float zone", PhD thesis, Université de Sherbrooke, Québec.

Burden, R.L., Faires, D.J. and Reynolds, A.C. (1981), *Numerical Analysis*, 2nd ed., Prindle, Weber & Schmidt, Boston, MA.

Chang, C.E. and Wilcox, W.R. (1975), "Inhomogeneities due to thermocapillary flow in floating zone melting", *J. Crystal Growth*, Vol. 28, pp. 8-12.

Chang, C.E. and Wilcox, W.R. (1976), "Analysis of surface tension driven flow in floating zone melting", *Int. J. Heat Mass Transfer*, Vol. 19 No. 3, pp. 355-66.

Chun, Ch.H. (1980), "Marangoni convection in a floating zone under reduced gravity", *J. Crystal Growth*, Vol. 48, pp. 600-10.

Chun, Ch.H. and Wuest, W. (1979), "Flow phenomena in rotating floating zones with and without Marangoni convection", *Proc. 3rd European Symp. on Materials and Fluid Sciences in Space, ESA SP-142*, pp. 283-8.

Chun, Ch.H. and Wuest, W. (1981), "Correlation of oscillations of flow and temperature in floating zone under microgravity", *Adv. Space Res.*, Vol. 1, pp. 17-20.

Chun, Ch.H. and Wuest, W. (1982), "Suppression of temperature oscillations of thermocapillary Marangoni convection in a floating zone by superimposing of rotating flows", *Acta Astronautica*, Vol. 9 No. 4, pp. 225-30.

Chun, Ch.H. and Wuest, W. (1983), "Free surface vibration of a floating zone induced by surface-tension-driven oscillating flow", *Proc. 4th European Symposium on Materials Sciences Under Microgravity, ESA SP-191*, pp. 205-11.

Duranceau, J. and Brown, R. (1986), "Thermal-capillary analysis of small-scale floating zone: steady-state calculations", *J. Crystal Growth*, Vol. 75, pp. 367-89.

Finn, R. (1986), *Equilibrium Capillary Surface*, Springer-Verlag, New York, NY, p. 245.

Jordan, A.S., Caruso, R. and Von Neida, A.R. (1980), "A thermoelastic analysis of dislocation generation in pulled Ga as crystals", *The Bell System Tech. Journal*, Vol. 59 No. 4, pp. 593-637.

Kazarinoff, N.D. and Wilkowski, J.S. (1990), "Marangoni flows in a cylindrical liquid bridge of silicon", in Roux, B. (Ed.) *Numerical Simulation of Oscillatory Convection in Low Pr Fluids*, Vieweg, Braunschweig, pp. 65-73.

Kobayashi, N. (1988), "Steady convection caused by the temperature inhomogeneity in a cylindrical floating zone", *Jpn. J. Appl. Phys.*, Vol. 27, pp. 20-4.

Kozhoukharova, Zh. and Slavchev, S. (1986), "Computer simulation of the thermocapillary convection in a non-cylindrical floating zone", *J. Crystal Growth*, Vol. 74, pp. 236-46.

Lai, C.L. (1984), "Studies of thermocapillary oscillation phenomena", PhD thesis, Case Western Reserve University, Cleveland, OH.

Lan, C.W. and Kou, S. (1990), "Thermocapillary flow and melt/solid interfaces in floating zone crystal growth under microgravity", *J. Crystal Growth*, Vol. 102, pp. 1043-58.

Lan, C.W., Kim, Y.J. and Kou, S. (1990), "Half-zone study of Marangoni convection in floating zone crystal growth under microgravity", *J. Crystal Growth*, Vol. 104 No. 4, pp. 801-8.

Nguyen, C.T., Bazzi, H. and Orfi, J. (1995a), "Numerical investigation of the effects of rotation on a germanium float zone under microgravity conditions", *Numerical Heat Transfer*, Vol. 28 No. 6, pp. 667-85.

Nguyen, C.T., Orfi, J. and Bazzi, H. (1995b), "Transient behavior of a $NaNO_3$ float zone operating at high Marangoni number under μ-g Conditions", *Numerical Heat Transfer*, Vol. 28 No. 3, pp. 299-320.

Pfann, W.G. (1966), *Zone Melting*, 2nd ed., Wiley, New York, NY.

Patankar, S.V. (1980), *Numerical Heat Transfer and Fluid Flow*, Hemisphere, Washington, DC.

Patankar, S.V. (1996), "Innovative research Inc. micro-compact V. 4.0", *Reference Manual*, Maple Grove, MN..

Preisser, F., Schwabe, D. and Sharmann, A. (1983), "Steady and oscillatory thermocapillary convection in liquid columns with free cylindrical surface", *J. Fluid Mech.*, Vol. 126, pp. 545-67.

Rupp, R., Müller, G. and Neumann, G. (1989), "Three-dimensional time-dependent modeling of the Marangoni convection in zone melting configuration of GaAs", *J. Crystal Growth*, Vol. 97 No. 1, pp. 34-41.

Saghir, M.Z. (1987), "A study of the Marangoni convection on the germanium float zone", *Low Gravity Sciences*, Vol. 67, Sciences and Technologies Series, Amer. Astronautical Society AAS 86-554, pp. 77-100.

Saghir, M.Z. (1988), "High purity germanium float zone modeling report", CAL Rept. 388A-1012, Canadian Space Agency, Ottawa, Ontario.

Saghir, M.Z. and Rosenblat, S. (1990), "Marangoni convection on a germanium float zone", *Microgravity Q.*, Vol. 1, pp. 19-29.

Saghir, M.Z., Hirata, A. and Nishizawa, S. (1992), "Experimental and numerical results of silicon oil column in earth environment", *Proc. 8th Int. Symp. on Space Tech. and Sci.*, Kagoshima, pp. 2193-8.

Schwabe, D., Scharmann, A., Preisser, F. and Oeder, R. (1978), "Experiments on surface tension driven flow in floating zone melting", *J. Crystal Growth*, Vol. 43, pp. 305-12.

Schwabe, D., Scharmann, A. and Preisser, F. (1979), "Steady and oscillatory Marangoni convection in floating zone under 1-g", *Proc. 3rd European Symp. on Material Science in Space*, Grenoble.

Schwabe, D. and Sharmann, A. (1979), "Some evidence for the existence and a magnitude of a critical Marangoni number for the onset of oscillatory flow in crystal growth melts", *J. Crystal Growth*, Vol. 46, pp. 125-31.

Schwabe, D., Preisser, F. and Scharmann, F. (1982), "Verification of the oscillatory state of thermocapillary convection in floating zone under low gravity", *Acta Astronautica*, Vol. 9 No. 4, pp. 265-73.

Schwabe, D. and Sharmann, A. (1983), "Measurement of the critical Marangoni number in a floating zone under reduced gravity", *Proc. 4th European Symp. on Material Science under Microgravity*, Spain, pp. 213-18.

Schwabe, D. and Scharmann, A. (1984), "Microgravity experiments on the transition from laminar to oscillatory thermocapillary convection in floating zones", *Adv. Space Res.*, Vol. 4 No. 5, pp. 43-7.

Schwabe, D. (1988), "Surface-tension-driven flow in crystal growth melts", *Crystals*, Vol. 11, pp. 75-112.

Schwabe, D., Lamprecht, R. and Sharmann, A. (1989), "Experiments on steady and oscillatory thermocapillary convection in space with applications to crystal growth", in Velarde, M.G. (Ed.), *Physico-Chemical Hydrodynamics: Interfacial Phenomena*, Plenum, New York, NY, pp. 291-310.

Schwabe, D., Velten, R. and Sharmann, A. (1990), "The instability of surface tension driven flow in models for floating zones under normal and reduced gravity", *Acta Astronautica*, Vol. 99, pp. 1258-64.

Slavchev, S.G. and Kojukharova, J.D. (1984), "Computer simulation of convection in floating zone melting", *Arch. Mech.*, Vol. 36, pp. 241-50.

Takao, A. (1985), "Crystal fabrication", in Einspruch, N.G. and Huff, H. (Eds), *VLSI Electronics Microstructure Sciences*, Vol. 12, Academic Press, New York, NY.

Wilcox, W.R. (1991), "Floating zone melting of electronics materials in space", *Proc. 29th AIAA Conf.*, Paper no. AIAA-91-0507.

Appendix. Boundary conditions on the free surface

The coordinate system (r′, z′), which is locally attached to the deformed free surface of the zone, is chosen as follows: (see Figure A1)

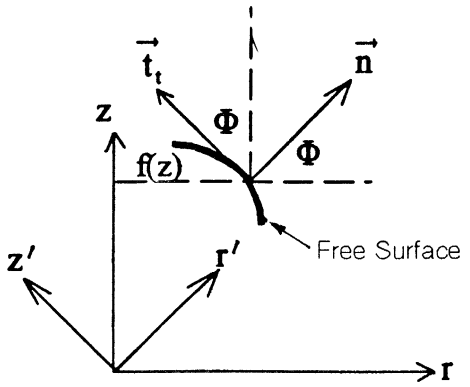

Figure A1.
Relationship between (r, z) and (r′, z′) coordinate systems

(r′, 0) is normal to the free surface, and (0, z′) is tangential to the free surface
The unit vector $\vec{t_t}$ is written as:

$$\vec{t}_t = \frac{-\sin\Phi\,\vec{r} + \cos\Phi\,\vec{z}}{\sqrt{\cos^2\Phi + \sin^2\Phi}} = \frac{-tg\Phi\,\vec{r} + \vec{z}}{\sqrt{1 + tg^2\Phi}} = \frac{\left(\frac{\partial f}{\partial z}\right)\vec{r} + \vec{z}}{\sqrt{1 + \left(\frac{\partial f}{\partial z}\right)^2}} \tag{A.1}$$

where Φ is the angle between (r, z) and r′, z′). We have then the following unit vectors along the tangential and normal directions:

$$\vec{t}_t = \left(\frac{\left(\frac{\partial f}{\partial z}\right)}{\sqrt{1 + \left(\frac{\partial f}{\partial z}\right)^2}}, \qquad \frac{1}{\sqrt{1 + \left(\frac{\partial f}{\partial z}\right)^2}} \right) \tag{A.2}$$

and

$$\vec{n} = \left(\frac{1}{\sqrt{1 + \left(\frac{\partial f}{\partial z}\right)^2}}, \qquad \frac{-\left(\frac{\partial f}{\partial z}\right)}{\sqrt{1 + \left(\frac{\partial f}{\partial z}\right)^2}} \right) \tag{A.3}$$

Table AI resumes the relationships between (r′, z′) and (r, z):

a) Equilibrium of the normal-stress at the free surface
The balance of the normal-stress at the free surface may be expressed as follows based on the well-known Laplace's equation, see for example Finn (1986) and Lai (1984):

$$-(p - p_\infty + 2\mu\varepsilon_{r'r'} = -\sigma\left(\frac{1}{R_1} + \frac{1}{R_2}\right) \tag{A.4}$$

Table AI.
The relationships between (r′, \′) and r,z)

	r	z
r′	$l_1 = \cos r'r$	$n1 = \cos r'z$
z′	$l_2 = \cos z'r$	$n_2 = \cos z'z$

$$-(p-p_\infty)2\mu(-(1_1^2\varepsilon_{rr}+n_1^2\varepsilon_{zz}+2n_1 1_1\varepsilon_{zr}) = -\sigma\left(\frac{1}{R_1}+\frac{1}{R_2}\right) \tag{A.5}$$

where p_∞ is the ambient pressure; ε_{ij} are viscous stresses; R_1 and R_2 are the radii of curvature given as follows:

$$\frac{1}{R_1} = \left(\frac{-\frac{\partial^2 f}{\partial z^2}}{\left[1+\left(\frac{\partial f}{\partial z}\right)^2\right]^{3/2}}\right) \tag{A.6}$$

$$\frac{1}{R_2} = \left(\frac{1}{f\left[1+\left(\frac{\partial f}{\partial z}\right)^2\right]^{1/2}}\right) \tag{A.7}$$

After substitution, the equation (A.5) becomes:

$$p - p_\infty - \frac{2\mu_M}{\left[1+\left(\frac{\partial f}{\partial z}\right)^2\right]}\left[\frac{\partial v_r}{\partial r}+\left(\frac{\partial f}{\partial z}\right)^2\left(\frac{\partial v_z}{\partial z}\right)-\left(\frac{\partial f}{\partial z}\right)\left(\frac{\partial v_z}{\partial z}+\frac{\partial v_r}{\partial z}\right)\right] = \frac{\sigma_M}{\left[1+\left(\frac{\partial f}{\partial z}\right)^2\right]^{3/2}}\left[\frac{1+\left(\frac{\partial f}{\partial z}\right)^2}{f}-\frac{\partial^2 f}{\partial z^2}\right] \tag{A.8}$$

b) Equilibrium of tangential shear-stress at the free surface
We have:

$$2\mu\varepsilon_{r'z'} = \frac{\partial\sigma}{\partial z'} = -\left|\frac{\partial\sigma}{\partial t}\right|\left[(\nabla t).\vec{t}_t\right] \tag{A.9}$$

$$2\mu[1_1 1_2\varepsilon_{rr}+n_2 n_1\varepsilon_{zz}+(n_2 1_1+1_2 n_1)\varepsilon_{zr}] = -\left|\frac{\partial\sigma}{\partial t}\right|\left[(\nabla t).\vec{t}_t\right] \tag{A.10}$$

which can be developed as:

$$\frac{\partial f}{\partial z}2\mu_M\left[\frac{\partial v_r}{\partial r}-\frac{\partial v_z}{\partial z}\right]+\mu_M\left[1-\left(\frac{\partial f}{\partial z}\right)^2\right]\left[\frac{\partial v_z}{\partial r}+\frac{\partial v_r}{\partial z}\right] = -\left|\frac{\partial\sigma}{\partial t}\right|\left[1+\left(\frac{\partial f}{\partial z}\right)^2\right]^{1/2}\left[\frac{\partial f}{\partial z}\frac{\partial t}{\partial r}+\frac{\partial t}{\partial z}\right] \tag{A.11}$$

c) The kinematic condition
The following additional condition, which is often referred as the kinematic condition, and expressing that no mass flux is across the free surface, is written as:

$$(\vec{v} \,.\, \vec{n}) \;=\; 0 \tag{A.12}$$

or as:

$$\left[\frac{1}{\left[1 \;+\; \left(\frac{\partial f}{\partial z}\right)^{2}\right]^{1/2}}\right]\left(v_r \;-\; \frac{\partial f}{\partial z}\, v_z\right) \;=\; 0 \tag{A.13}$$

The above condition must also be fully satisfied during the course of numerical solution procedure.

d) The thermal boundary condition at the free surface

We assume that the free surface is adiabatic i.e. the heat loss to the surrounding environment is considered negligible. This condition is expressed as follows:

$$-(\lambda\, \vec{n}\, \nabla t) \;=\; 0 \tag{A.14}$$

or as:

$$-\lambda\left[\frac{1}{\left[1 \;+\; \left(\frac{\partial f}{\partial z}\right)^{2}\right]^{1/2}}\right]\left(\frac{\partial t}{\partial r} \;-\; \frac{\partial f}{\partial z}\,\frac{\partial t}{\partial z}\right) \;=\; 0 \tag{A.15}$$

e) The boundary conditions under dimensionless form

The above boundary conditions at the free surface, the equations A.8, A.11, A.13 and A.15, are rewritten respectively as follows under the dimensionless form:

$$\frac{CaMa}{Pr}\, P \;-\; BsZ \;-\; \frac{Ca}{\left[1 \;+\; \left(\frac{\partial F}{\partial Z}\right)^{2}\right]}\left[\frac{\partial V_R}{\partial R} \;+\; \left(\frac{\partial F}{\partial Z}\right)^{2}\left(\frac{\partial V_Z}{\partial Z}\right) \;-\; \left(\frac{\partial F}{\partial Z}\right)\left(\frac{\partial V_Z}{\partial R} \;+\; \frac{\partial V_R}{\partial Z}\right)\right]$$
$$= \frac{1}{\left[1 \;+\; \left(\frac{\partial F}{\partial Z}\right)^{2}\right]^{3/2}}\left[\frac{1 \;+\; \left(\frac{\partial F}{\partial Z}\right)^{2}}{F} \;-\; \frac{\partial^2 F}{\partial Z^2}\right] \tag{A.16}$$

$$2\,\frac{\partial F}{\partial Z}\left[\frac{\partial V_R}{\partial R} \;-\; \frac{\partial V_Z}{\partial Z}\right] \;+\; \left[1 \;-\; \left(\frac{\partial F}{\partial Z}\right)^{2}\right]\left[\frac{\partial V_Z}{\partial R} \;+\; \frac{\partial V_R}{\partial Z}\right] \;=\; -\left[1 \;+\; \left(\frac{\partial F}{\partial Z}\right)^{2}\right]^{1/2}\left[\frac{\partial F}{\partial Z}\,\frac{\partial T}{\partial R} \;+\; \frac{\partial T}{\partial Z}\right] \tag{A.17}$$

$$\frac{1}{\left[1 \;+\; \left(\frac{\partial F}{\partial Z}\right)^{2}\right]^{1/2}}\left(V_R \;-\; \frac{\partial F}{\partial Z}\, V_Z\right) \;=\; 0 \tag{A.18}$$

and

$$\frac{\partial T}{\partial R} - \frac{\partial F}{\partial Z}\frac{\partial T}{\partial Z} = 0 \tag{A.19}$$

From the above equations, some further simplifications may be introduced, for example in the case where Ca « 1 and $(\partial F / \partial Z)^2$ « 1, as adopted and discussed in the section "Boundary and initial conditions" of the paper.

f) On the determination of the position of the zone free surface

Under the simplifications Ca « 1 and $(\partial F / \partial Z)^2$ « 1, the equation of the normal-stress balance (A.16) becomes:

$$Ca\ Re_{th}\ P\ \ BsZ = \frac{1}{F} - \frac{\partial^2 F}{\partial Z^2} \tag{A.20}$$

Furthermore, for the static case corresponding to the non-heated zone i.e. $Re_{th} = Ma = 0$, the above equation becomes as follows:

$$-BsZ = \left[\frac{1}{F} - \frac{\partial^2 F}{\partial Z^2}\right] \tag{A.21}$$